European Journal of Materials

ISSN: 2688-9277 (Online) Journal homepage: www.tandfonline.com/journals/tems20

Adapting an in situ X-ray CT compression stage for pull-out testing: Methodological development and characterization of failure evolution in Ni/PU hybrid foams

Jonas Fell, Hendrik Jost , Dionne Schnubel , Maurice Großelindemann , Marius Weiler , Anne Jung & Hans-Georg Herrmann

To cite this article: Jonas Fell, Hendrik Jost , Dionne Schnubel , Maurice Großelindemann , Marius Weiler , Anne Jung & Hans-Georg Herrmann (2026) Adapting an in situ X-ray CT compression stage for pull-out testing: Methodological development and characterization of failure evolution in Ni/PU hybrid foams, European Journal of Materials, 6:1, 2669894, DOI: 10.1080/26889277.2026.2669894

To link to this article: https://doi.org/10.1080/26889277.2026.2669894

Published online: 17 Jun 2026.

EUROPEAN JOURNAL OF MATERIALS
2026, VOL. 6, NO. 1, 2669894
https://doi.org/10.1080/26889277.2026.2669894

Taylor & Francis
by informa

STRUCTURAL MATERIALS

OPEN ACCESS Check for updates

Adapting an in situ X-ray CT compression stage for pull-out testing: Methodological development and characterization of failure evolution in Ni/PU hybrid foams

Jonas Fell[a,b], Hendrik Jost[b], Dionne Schnubel[b], Maurice Großelindemann[c], Marius Weiler[b], Anne Jung[d] and Hans-Georg Herrmann[a,b,e]

[a]Center for Correlative Microscopy & Tomography CoMiTo, Faculty of Natural Sciences and Technology, Saarland University, Saarbrücken, Germany; [b]Lightweight Systems, Materials Science, Faculty of Natural Sciences and Technology, Saarland University, Saarbrücken, Germany; [c]Fichtner & Schicht GmbH, Schlangen, Germany; [d]Protective Systems, Helmut-Schmidt University/University of the Federal Armed Forces Hamburg, Hamburg, Germany; [e]Fraunhofer Institute for Nondestructive Testing IZFP, Saarbrücken, Germany

ABSTRACT
The integration of metallic fasteners into cellular hybrid materials presents significant challenges regarding interface integrity and localized load transfer. This study is exploratory in nature, focusing on the methodological development and evaluation of a custom-engineered in situ pull-out system designed for X-ray micro-computed tomography (micro-CT). By successfully adapting an existing compression stage for pull-out configurations, this research enables the three-dimensional visualization of internal failure sequences that remain inaccessible via conventional testing methods. The investigation of Nickel-coated polyurethane (PU) hybrid foams demonstrated a matrix collapse stress of 7.1 MPa in compression mode and a pull-out resistance of 4 MPa. In situ analysis revealed that compression failure is driven by localized deformation bands oriented at 10° to 15°, likely attributable to structural inhomogeneities. During pull-out, interfacial bonding remains intact beyond initial matrix failure, forming an annular damage zone characterized by progressive strut buckling and lateral sliding. Based on these findings, we propose design guidelines that a larger major diameter and coarser thread pitch enhance load-bearing capacity and preserve structural integrity. These insights underscore the potential of Ni/PU hybrids as tunable, high-performance materials for sustainable infrastructure.

ARTICLE HISTORY
Received 19 December 2025
Revised 14 April 2026
Accepted 1 May 2026

KEYWORDS
In situ X-ray computed tomography; metal hybrid foam; pull-out test; cellular material; mechanical testing

Introduction

Metallic foams constitute a distinctive class of cellular materials characterized by a porous architecture that combines low density with exceptional mechanical, thermal, and functional properties. Their high strength-to-weight ratio, tunable stiffness, and excellent thermal conductivity make them particularly attractive for lightweight structural components, multifunctional load-bearing elements, and efficient heat dissipation systems (Banhart, 2001; Gibson, 2000). In the context of green civil engineering, these materials address the urgent need for resource-efficient construction by offering a high-performance alternative to energy-intensive monolithic metals and heavy concrete elements. From a sustainability perspective, the use of metallic foams as lightweight materials offers substantial potential for reducing raw material consumption and associated greenhouse gas emissions over the entire life cycle of structural systems (Ceci et al., 2025). Unlike traditional cellular materials, the hybrid nature of coated foams allows for a strategic optimization of the material-specific carbon footprint, as structural performance is achieved with significantly reduced metallic mass. By enabling mass reduction without compromising structural integrity or safety, metallic foams contribute directly to resource-efficient design strategies and support the development of green civil engineering materials aligned with climate-neutral construction goals.

CONTACT Jonas Fell jonas.fell@uni-saarland.de Center for Correlative Microscopy & Tomography CoMiTo, Faculty of Natural Sciences and Technology, Saarland University, Campus E3 1, 66123 Saarbrücken.
This article has been corrected with minor changes. These changes do not impact the academic content of the article.

A key advantage of metallic foams lies in their outstanding energy absorption capability under both quasi-static and dynamic loading conditions. This property renders them highly suitable for impact- and blast-resistant structures, where controlled deformation and progressive collapse mechanisms are critical for mitigating extreme loads. In the automotive and aerospace industries, metallic foams have already demonstrated significant benefits in crashworthiness applications, where they enhance occupant safety while simultaneously reducing vehicle mass and fuel consumption (Ashby et al., 2001; Lefebvre et al., 2008). Beyond these established sectors, metallic foams are increasingly considered for protective systems in civil and defense-related applications, including blast walls, facade elements, sacrificial cladding, and sandwich core structures designed to withstand explosions, projectile impacts, and shock waves. Their ability to dissipate large amounts of kinetic energy, reduce peak forces, and limit damage propagation makes them highly promising materials for resilient infrastructure and critical protective systems (Wu et al., 2024).

In the context of sustainable and resilient construction, metallic foams offer a compelling combination of mechanical performance, durability, and recyclability. As metallic materials, they can be fully recycled at the end of their service life, further strengthening their role in circular economy concepts for civil engineering. To fully exploit their macroscopic performance, it is essential to understand the underlying deformation and failure mechanisms governing their behavior. Consequently, alongside extensive macroscopic mechanical investigations, increasing attention has been devoted to the detailed study of individual foam struts. These microscale analyses provide fundamental insights into local deformation modes, damage initiation, and fracture mechanisms, which are crucial for developing reliable predictive models and optimizing metallic foams for demanding impact and blast protection applications (Jung et al., 2018; Luksch et al., 2021; Reis et al., 2020).

Micro-CT has emerged as a key tool for non-destructive characterization of foam morphology, cell topology, and internal defects, providing high-resolution 3D data that serve as essential input for computational modeling, digital twins, and physics-based simulation frameworks (Betts et al., 2014; Kaya et al., 2019; Leblanc et al., 2022). Beyond static imaging, in situ X-ray computed tomography has increasingly been integrated with mechanical loading rigs to capture real-time, three-dimensional deformation and damage evolution under controlled stress states. This approach enables direct correlation of microstructural mechanisms with the macroscopic mechanical response, enhancing understanding of collapse modes, strut buckling, cell wall fracture, and energy dissipation pathways.

To date, mechanical in situ experiments using CT have been reported for a wide range of materials. For example, recent work by Wang et al. employs in situ CT to investigate progressive compaction and crack initiation in fiber-reinforced concrete and cementitious composites under quasi-static loading, linking microstructural changes directly to stress–strain behavior and effective stiffness degradation (Wang et al., 2025; 2025; 2025; Wang & Lu, 2026). The versatility of in situ CT is not limited to compression; tensile and bending rigs have also been integrated with high-flux X-ray sources to observe failure processes in various structures and composites. For instance, Wingate et al. performed in situ CT during flexure test of tape-laminate composites, capturing crack propagation and interfacial delamination (Wingate & Czabaj, 2022). A further case in point is the investigation of fiber-reinforced thermoplastic composites, where stress relaxation significantly influences the experimental procedure (Maurer et al., 2022). Furthermore, digital volume correlation (DVC) techniques have been integrated with CT to quantify full-field strain distributions in three dimensions, greatly enhancing the fidelity of constitutive model calibration (Wang et al., 2025). Complementary in situ methodologies include synchrotron-based high-speed tomography, which achieves temporal resolutions on the order of milliseconds, enabling observation of strain localization and fracture propagation under dynamic impact loading (Song et al., 2022; Wu et al., 2025). Taken together, in situ CT approaches deliver a powerful experimental platform to link morphology, microstructure evolution, and mechanical performance of metallic foams and related materials.

In the context of metallic foams and foam-based composites, in situ CT is limited to compression tests and have so far been applied mainly to aluminum foams to link microstructural evolution with macroscopic mechanical response (Fíla et al., 2016; Jung et al., 2018; Nogatz et al., 2024; Wang et al., 2023). Moreover, in situ tensile tests have been performed on single foam struts (Jung et al., 2018).

In parallel, hybrid systems such as nickel-coated polyurethane (Ni/PU) foams have been developed, with studies addressing manufacturing processes and heat treatments to enhance mechanical performance (Fries et al., 2024; Jung & Diebels, 2016; Kunz & Jung, 2022). However, systematic studies on Ni/PU hybrid foams, particularly in insert-reinforced or interface-critical configurations, are still lacking, leaving the behavior under complex loading conditions such as pull-out of embedded inserts insufficiently understood.

This study is part of a larger project dedicated to the development and characterization of Ni/PU hybrid foams for protective applications. Potential applications include mobile blast protection barriers for explosive ordnance disposal services and blast resistant facade elements designed to safeguard critical infrastructure, such as embassies and governmental buildings. To enable mechanical attachment and integration into such systems, threaded inserts must be incorporated into the foam structure without compromising its performance.

The primary objective of the presented work is to enable the investigation of mechanical behavior and damage mechanisms of metallic foams with and without integrated inserts using in-situ X-ray micro-CT. Given the explorative nature of this study, the analysis serves as a methodological demonstration, utilizing individual specimens to illustrate the potential of in-situ micro-CT for capturing fundamental failure sequences. A central pillar of this work is the development and implementation of a novel in-situ pull-out testing setup. Operating as a proof-of-concept, this setup was utilized to evaluate the bonding characteristics between the insert and the foam matrix under real-time observation. Two distinct configurations were investigated: (i) an in-situ compression test to characterize the foam's energy absorption, and (ii) the newly developed in-situ pull-out test. While the scope is limited to a representative single-specimen study for each case, these experiments provide 3D insights into the structural integrity and failure initiation of hybrid metallic foams, establishing a robust methodological framework for future large-scale testing.

Materials and methods

Ni/PU hybrid foam

The nickel-coated foams were fabricated by Fichtner & Schicht GmbH via an electrodeposition process designed to achieve uniform coating and structural stability of the porous substrate. Prior to electrodeposition, the polyurethane foam was rendered electrically conductive using a thin conductive pre-coating to ensure homogeneous current distribution throughout the open-cell structure. The prepared foam was then mounted in a stabilization frame, which maintained the geometry of the foam and prevented collapse during the initial phase of deposition.

The electrodeposition was carried out in a nickel electrolyte bath with dimensions of approximately $6000 \times 1500 \times 1600$ mm and a total volume of about 13.5 m^3. Depending on the specimen geometry, smaller laboratory-scale baths were used. The stabilization frame containing the foam was immersed in the bath, initiating the electrodeposition process. During the initial hours of the approximately 48-hour coating process, a thin nickel layer was deposited to provide mechanical stability while preserving the pore structure.

After this stabilization phase, the foam was removed from the stabilization frame and mounted into a coating frame for the main deposition step. In this phase, the nickel layer was grown to the desired thickness of 150 μm under controlled current density, which was adjusted according to the specimen size and target coating thickness. To ensure a uniform layer distribution, the coating frame was gently moved within the bath during deposition.

Once the desired coating thickness was reached, the foams were removed from the electrolyte, rinsed thoroughly with deionized water to remove any remaining residues, and dried at ambient conditions.

For the fabrication of insert-reinforced specimens, multiple commercial insert nuts were first fully embedded into open-cell PU foam panels of approximately $250 \times 250 \times 20$ mm. The steel inserts utilized in this study featured an M8 internal thread and a specialized external geometry with total length of 15 mm. The external thread profile was characterized by a minor diameter of 11.5 mm, a pitch diameter of 12.5 mm, and a major diameter of 13.5 mm. The selection of these standardized components was driven by economic efficiency and to ensure the industrial scalability of the process. Furthermore, the use of conventional steel threaded inserts ensures high versatility for the final protection system, as it allows for the straightforward and secure attachment. Building on this explorative work, subsequent studies are planned to systematically evaluate a broader range of steel threaded inserts in the future to optimize bonding performance and load-bearing capacity.

After embedding the inserts into the foam panels, the preforms underwent Ni coating following the same electrodeposition procedure described above, thereby coating both the foam skeleton and the inserts within one integrated process. The fabrication is schematically visualized in Figure 1.

To ensure representativeness of the continuum mechanical properties and to minimize size effects, a minimum of 4–8 pores must be contained in every direction within each foam specimen, as suggested by prior studies (Ashby et al., 2001; Bastawros et al., 2000). This condition is satisfied with a lateral extension of approximately 20 mm for the 20 ppi foam and 40 mm for the 10 ppi foam (Bronder et al., 2025; Jung & Diebels, 2017). Based on this requirement two specimen geometries were prepared for the experimental investigations.

For in-situ compression tests, a 20 ppi cylindrical specimen with a diameter of 25 mm and a height of 20 mm were extracted from the coated foam plates (Figure 2(a)). For in-situ pull-out tests, a 10 ppi cubic specimen with lateral dimensions of 40 × 40 mm and a height of 20 mm were prepared, each containing a centrally positioned insert (Figure 2(b)). The specimens geometries are precisely extracted

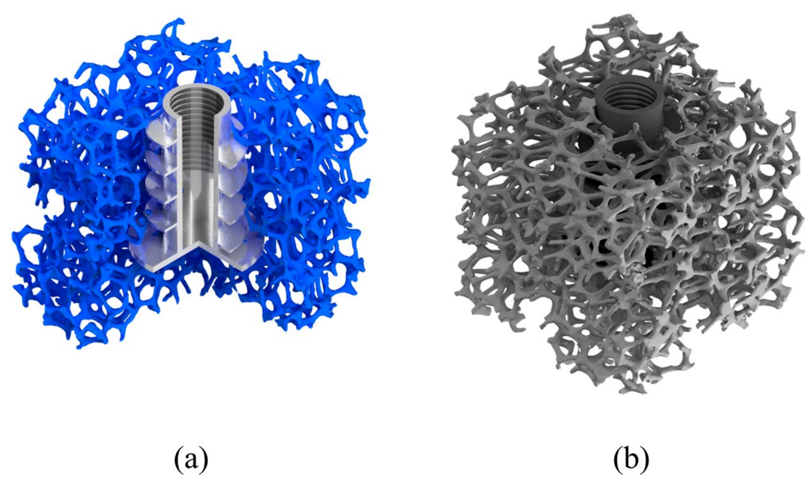

Figure 1. Schematic visualization of the fabrication of a single insert-reinforced specimen. (a) First, insert is embedded in PU foam. (b) Second, foam and insert are coated with Ni via electrodeposition.

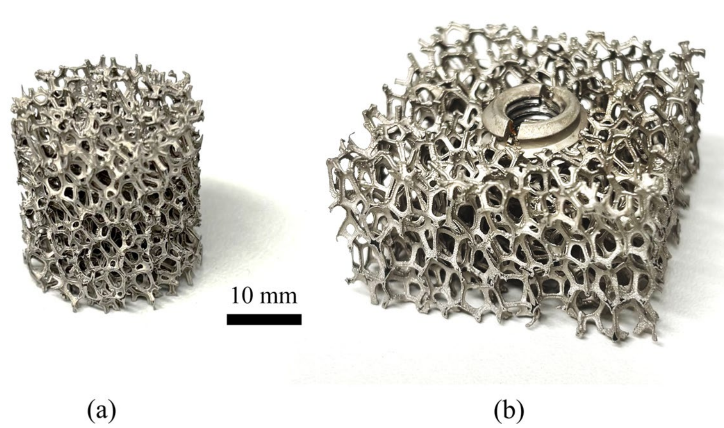

Figure 2. (a) Cylindrical specimen for compression test and (b) cubic specimen with insert for pull-out test.

using a waterjet cutting system to minimize thermal or mechanical damage. Additionally, the top and bottom surfaces were briefly ground to obtain a flat contact area on each.

Both specimen types were analyzed using X-ray computed tomography (CT) to characterize the internal structure, and the integrity of the insert–foam interface prior to and during mechanical loading.

X-ray micro-computed tomography

X-ray CT is a non-destructive imaging technique that reconstructs the internal structure of a specimen from a series of X-ray projection images taken at different rotation angles. A system based on geometrically magnification consists of an X-ray source, a rotational stage holding the specimen, and a flat-panel detector that records the transmitted radiation. By computationally reconstructing the acquired projections, a three-dimensional (3D) representation of the material's internal morphology can be obtained (Fernandes et al., 2021; Fell et al., 2023a). Image contrast arises from differences in X-ray attenuation, which depend on the material's density and atomic composition. The magnification of the image depends on the relative distances between the X-ray source, the object, and the detector (focus-object distance (FOD) and focus-detector distance (FDD)), allowing the spatial resolution to be tailored to the specimen size. Moreover, X-ray CT enables in-situ analysis of microstructures and their evolution during mechanical testing, providing detailed insights in 3D (Fell et al., 2023b).

To characterize the internal structure of the specimens an X-ray micro-CT called CT-alpha from ProCon X-ray GmbH was used in this study. The setup consists of an X-ray microfocus-source (up to 160 kV), a high-resolution flat panel detector (Teledyn Shadowbox), and a rotation stage enabling full 360° scans. The sample was positioned at an appropriate FOD and to achieve the desired magnification, resulting in a voxel size of approximately 45 µm.

During each scan, a series of 1400 radiographic projections were acquired over a full rotation of 360°, with an exposure time of 1500 ms per projection using 160 kV tube voltage. The data were reconstructed using a filtered back projection algorithm to obtain a three-dimensional grayscale volume.

Micro-CT enables non-destructive, three-dimensional imaging of the specimen's internal microstructure with micrometer-scale resolution. This allows visualization and quantification of features such as pore morphology, strut thickness, coating uniformity, and potential defects. In the present study, micro-CT was used to evaluate the structural integrity of the nickel-coated hybrid foam, and to identify failure mechanisms.

In-situ device

A Deben CT5000 in-situ mechanical testing stage (Deben UK Ltd.) was used for all experiments conducted inside the micro-CT system. As shown in Figure 3(a), the CT5000 is a servo-mechanical loading device primary designed for in-situ compression and tension experiments under tomographic observation. It allows the application of precise, computer-controlled load or displacement sequences while maintaining compatibility with the rotational geometry of the micro-CT scanner. The system operates with a maximum load capacity of 5 kN and offers micrometer displacement resolution, enabling highly accurate control of deformation processes.

For compression testing, the stage was equipped with parallel stainless steel plates ensuring homogeneous load distribution and minimal alignment error, as illustrated in the radiographic image in Figure 3(b). A constant movement of 0.5 mm per minute was applied during the compression. During the test, the specimen deformation was continuously monitored through sequential tomographic scans, allowing the correlation between global mechanical response and local microstructural evolution. This setup enables a non-destructive and time-resolved investigation of deformation and damage mechanisms in metallic foams.

To extend the functionality of the CT5000 and investigate insert–foam interfaces, the stage was adapted for pull-out testing. The setup illustrated in Figure 4, consists of four columns that transmit the load, corresponding to the load frame of a conventional tensile testing machine. On the columns rests a support plate equipped with two bars, each 10 mm wide and 40 mm long, on which foam

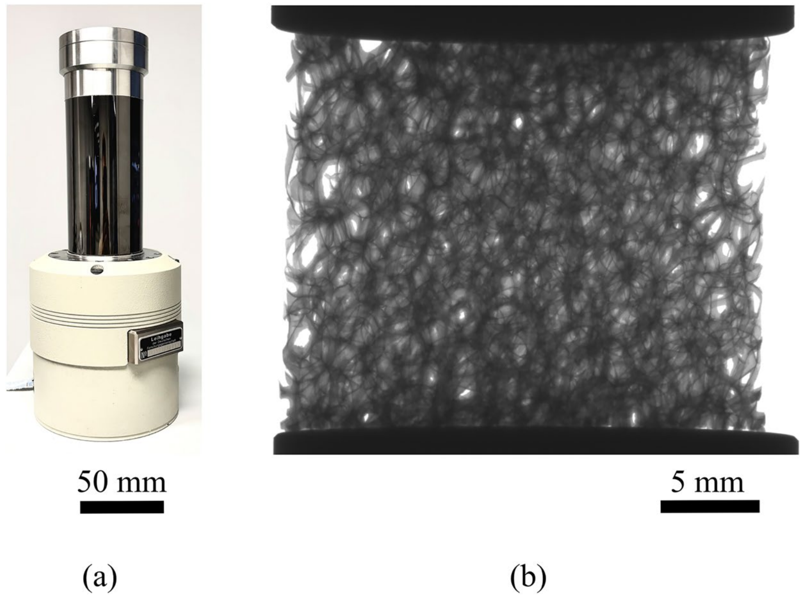

Figure 3. (a) Deben CT-5000 and (b) radiography of the foam being compressed between two hardened steel compression plates.

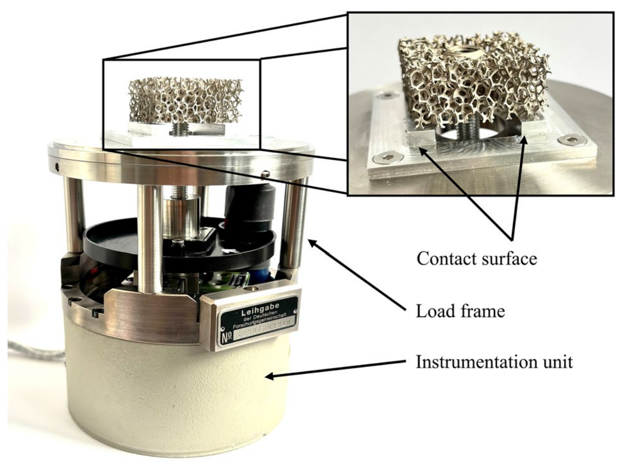

Figure 4. Setup for pull-out tests: The threaded rod screwed into the insert is pulled downward out of the foam.

specimens of 40×40 mm are placed. In the center of the support plate, a borehole allows the threaded rod with the insert to be pulled downward during testing. Through the specific design of the setup and the use of high-strength aluminum for the threaded rod and support plate, X-ray attenuation was minimized, ensuring optimal image quality during tomographic observation.

The modified setup enables controlled pull-out of embedded inserts under tomographic observation, allowing detailed assessment of interfacial debonding and local damage initiation. Using both compression and pull-out configurations on the same in-situ platform ensures consistent conditions and enables direct comparison of bulk and interfacial mechanical behavior. All tests were conducted inside the ProCon CT-alpha, with sequential scans reconstructed and analyzed to track crack initiation and interfacial failure during loading.

For both experimental setups, a baseline scan was performed in the initial, unloaded state prior to the commencement of mechanical testing. During the in-situ procedure, the first scan under load was strategically timed to capture the state just prior to reaching the peak load, followed by a subsequent scan immediately after the peak load to visualize the onset of structural failure. In the case of the compression tests, an additional measurement was conducted within the plateau regime to observe the progressive cell collapse. Both experiments concluded with a final scan at the end of the mechanical test to document the ultimate damage state.

Results

In-situ compression test

The in-situ compression test reveals the characteristic deformation behavior of metallic foams, as shown in the force-displacement diagram in Figure 5. The initial stage of the force – displacement curve exhibits a linear elastic response up to the collapse strength, represented by a distinct force maximum (see CT1 in Figures 5 and Wu et al., 2024(a)). This stage corresponds to the uniform elastic deformation of the foam's cell walls, where the structural integrity of the porous network remains intact.

A peak load (F_{max}) of 3494 N, reached at a displacement of 0.5 mm at the so called plastic collapse was identified immediately prior to the first significant force drop, marking the onset of structural failure. The corresponding plastic collapse stress (σ_{pl}) was calculated by normalizing this peak load against the initial cross-sectional area (A_0) of the specimen:

$$\sigma_{pl} = F_{max} / A_0 = F_{max} / (\pi \cdot r^2) \tag{1}$$

Using the specimen radius (r) of 12.5 mm, the calculation yields a plastic collapse stress of 7.1 MPa. This value serves as the primary indicator for the load-bearing capacity of the Ni/PU hybrid foam under compressive loading.

The plastic collapse is followed by a sharp force drop of about 3 kN (CT2 and CT3), which correlates to the localized fracture of individual struts and the development of collapse bands. These structural changes define the transition into the subsequent deformation region. During the plateau phase (beyond CT3), the force raises progressively constant while displacement increases, indicating sequential failure and densification of the cellular network.

Beyond CT4 (see Figures 5 and Wu et al., 2024(b)), densification is predominantly observed, where remaining pores progressively close and the structure compacts. This leads to a steeper increase in the applied force, as the deformation mechanism transitions from cell wall bending and buckling to plastic deformation and work hardening of the solid skeleton. At this stage (see CT5 in Figures 5 and Wu et al., 2024(c)), the material behavior increasingly resembles that of bulk nickel, as porosity and compressibility are largely eliminated.

To further elucidate the failure mechanism, Figure 7(a) presents a reconstructed CT cross-section revealing localized densification along a shear plane inclined at 10°–15°. This structural characteristic is confirmed across the entire sample volume via the standard deviation of a Z-projection (see Figure

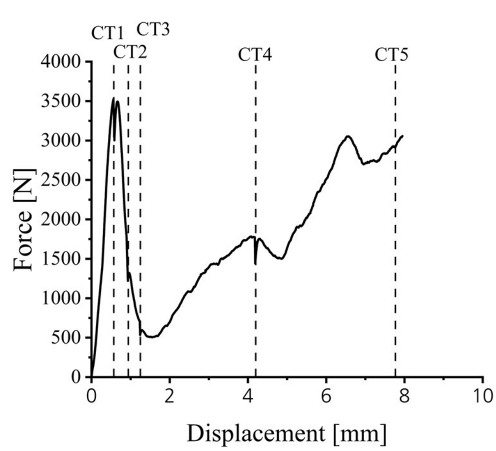

Figure 5. Force-displacement curve of the compression test. The specimen exhibits a peak force of approximately 3.5 kN at 0.5 mm displacement, indicating plastic collapse. Following a significant force drop to 0.5 kN, a stable plateau regime is observed, with densification-induced hardening initiated at a displacement of approximately 2 mm. Multiple CT scans were performed as marked in the diagram.

7(b)). The projection, generated using Fiji, superimposes the individual slices to highlight the volumetric consistency of the observed densification (Schindelin et al., 2012).

Further evaluation of the mechanical properties, utilizing a statistically significant amount of specimens, will be addressed in future research to ensure the robustness and reproducibility of the data.

In-situ pull-out tests

The force– displacement curve (Figure 8) obtained from the pull-out test on the Ni/PU hybrid foam with embedded inserts reveals several distinct deformation stages. In the initial linear region, the

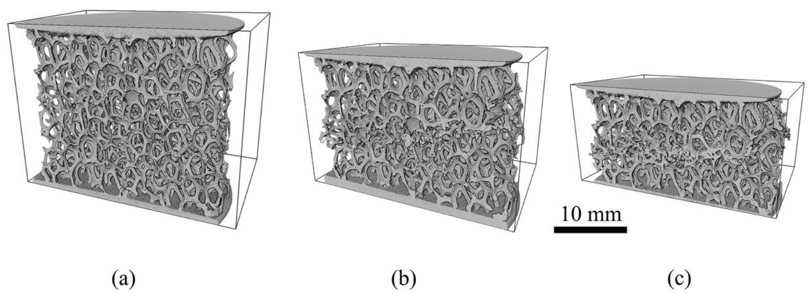

Figure 6. CT results are represented as a 3D cutaway view of the reconstructed volume, showing the internal architecture through a longitudinal clipping plane. The subfigures represent specific loading states: (a) specimen state CT1, (b) state CT4, and (c) state CT5, as referenced in the curve in Figure 5. Gradually collapse of cellular structure preferentially along a 10° to 15° shear plane and clearly visible densification.

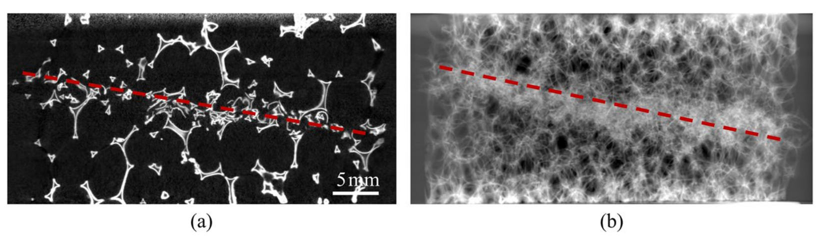

Figure 7. (a) Reconstructed CT cross-section exhibiting the compressed pore structure along a 10°–15° plane. (b) Standard deviation of Z-projection (processed in Fiji) representing a superposition of all planes in the orientation shown in (a). This method visualizes the structural characteristics throughout the entire volume and confirms a consistent densification along the 10°–15° plane (same scale).

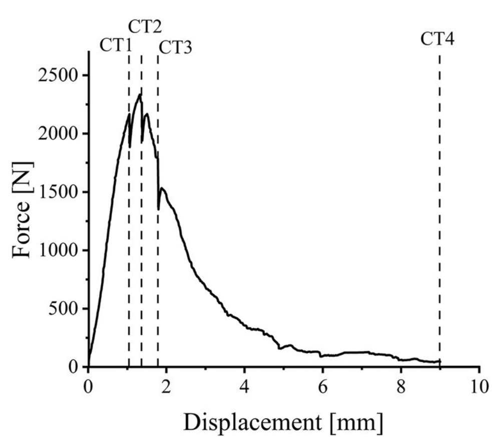

Figure 8. Load-displacement behavior during pull-out testing. The curve exhibits a peak load of approximately 2.3 kN at a displacement of 1.5 mm, followed by a distinct force drop. Markers indicate the specific displacement steps at which interrupted CT scans were performed to capture structural changes.

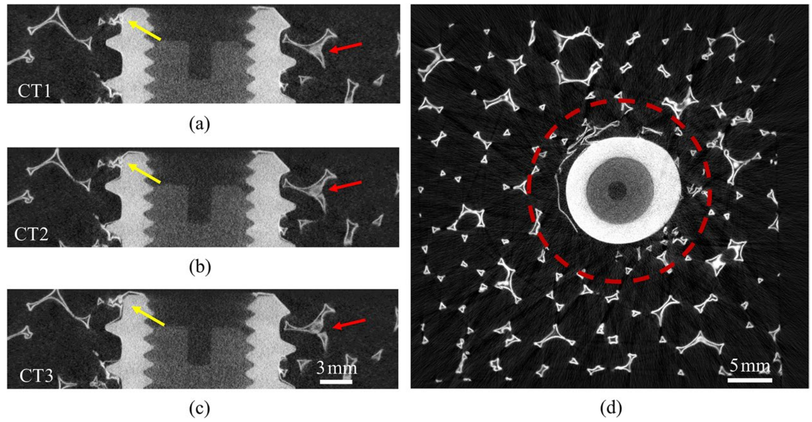

Figure 9. Evolution of structural failure during in situ testing. Comparison of reconstructed CT slices at time frame (a) CT1, (b) CT2, and (c) CT3 reveals the fracture of individual struts (red arrows) and delamination at the interface between the insert coating and the substrate (yellow arrows) at the top of the insert. (d) Visualization of the annular damage zone, highlighting the characteristic failure volume within the marked ring.

response is governed by the elastic deformation of the surrounding foam structure, indicating effective load transfer from the insert to the metallic network. No detectable damage is observed in the CT during this phase, which can be seen in the reconstructed slice of the time frame CT1 in Figure 9(a). The image illustrates the threaded section within the insert and the adjacent foam matrix surrounding it, showing no visible damage.

Upon reaching the peak load of approximately 2.3 kN at a displacement of 1.3 mm, the initial fracture of cell struts occurs. Notably, this failure is not initiated at the foam-insert interface; instead, it occurs a certain distance from the insert, as confirmed by the corresponding time frames CT2 and CT3 (see Figures 8 and Reis et al., 2020(b,c)). This marks the onset of damage and results in a noticeable drop in force. As illustrated in Figure 9(d), a characteristic damage volume forms an annular pattern around the insert within a distance of approximately 5 mm.

Coincident with the force drop, localized delamination between the nickel coating and the underlying insert is observed, indicating interfacial shear stresses exceeding the adhesion strength of the coating. However, the struts connected to the insert remain intact, demonstrating strong mechanical interlocking and effective adhesion between the insert coating and the metallic framework.

With increasing displacement, the damage evolves progressively as additional struts fracture, leading to a partial collapse of the cellular structure within a defined zone around the insert. Simultaneously, localized delamination between the nickel coating and the steel surface occurs, marking a loss of interfacial adhesion. As the insert is gradually pulled out, several struts remain geometrically attached and mechanically interlocked with the thread geometry, undergoing partial bending as illustrated by the comparison of the 3D models from CT time frames CT1 and CT4 in Figure 10. This stage is characterized by a continuous force decay, corresponding to the sequential loss of load-bearing struts, the interfacial debonding at the insert surface, and the gradual reduction of the effective contact area.

The normalized pull-out resistance defined as the apparent interfacial shear strength (τ), was calculated by dividing the peak load (F_{max}) by the nominal contact area between the insert and the foam (A_{int}) (Herrera-Franco & Drzal, 1992; Pech-Can et al., 2024):

$$\tau = F_{max} / A_{int} = F_{max} / (\pi \cdot d \cdot L_{emb}) \qquad (2)$$

Although failure was observed to initiate within the bulk foam at a radial distance of 5 mm, the interface area remains the standard reference for evaluating the load-bearing capacity of the hybrid connection. Based on a peak load of 2334 N and a nominal contact area of 589.05 mm^2 (determined by the insert pitch diameter of 12.5 mm and an embedding length of 15 mm), the calculated resistance is 3.96 MPa.

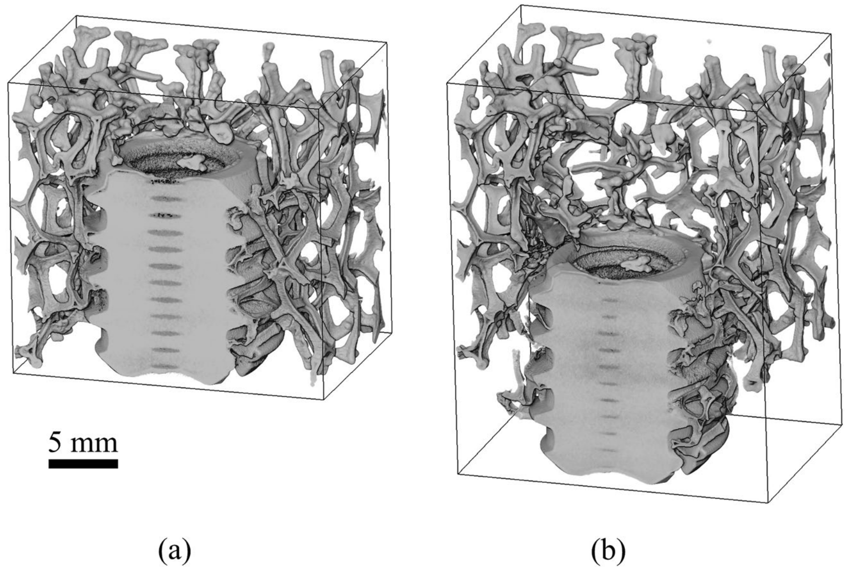

Figure 10. Cropped 3D visualizations of the pull-out specimen at (a) the initial state (CT1) and (b) the final state (CT4) after 9 mm displacement. The post-test view reveals that while the Ni-coating and struts remain geometrically attached, localized delamination indicates a loss of interfacial adhesion. Failure is primarily driven by bulk strut collapse within a characteristic annular damage zone, rather than a complete foam–insert debonding.

Discussion

The integration of fasteners into low-density cellular materials remains a significant challenge, as the porosity of foams often leads to premature failure at highly stressed interfaces. This study addresses this problem by investigating hybrid nickel-coated polymer foams using a custom-adapted in situ compression stage which enabled both uniaxial compression tests and pull-out experiments under X-ray monitoring. Initially, the fundamental mechanical behavior of the hybrid foam matrix was characterized through uniaxial compression. Subsequently, pull-out tests were performed, with a specific focus on investigating the highly stressed transition zones between the metallic insert and the hybrid foam framework.

This baseline characterization in compression mode revealed that the hybrid foam matrix exhibits a collapse stress of approximately 7 MPa. This mechanical response was characteristically defined by a failure localized along a shear plane oriented at 10° to 15° relative to the loading axis (see Figure 6 and 7). In an ideal isotropic material, the failure zone would be expected to align perpendicular to the deformation zone (Jung & Diebels, 2019). However, due to structural defects and inherent inhomogeneities in the nickel coating thickness, a significant deviation from these theoretical planes occurs, leading to the formation of localized deformation bands (Banhart, 2001; Bastawros et al., 2000). The resulting concentration of deformation into these inclined crush bands indicates that the effective load-transfer zone is restricted to a narrow region, where initial cell wall buckling is succeeded by lateral sliding rather than uniform axial compaction.

In the pull-out tests, damage did not initiate at the insert interface. Instead, the fracture of individual struts in specific distance to the insert was observed first, followed by localized delamination of the Ni-coating from the steel insert (see Figure 9). The electrochemical coating process ensures a homogeneous, closed Ni-layer on the insert that is metallurgically integrated with the adjacent foam struts. This configuration exhibits superior stability compared to the individual struts within the bulk foam, effectively shifting the structural weak point into the surrounding matrix. This resulted in a characteristic annular damage zone approximately 5 mm from the insert surface (see Figure 9(d)). The calculated pull-out resistance of approximately 4 MPa represents a lower bound for the actual interfacial strength, as CT observations confirm that failure occurred in the bulk material rather than the bond line.

From a design perspective, these findings suggest that coating homogeneity and the intrinsic microstructure of the foam are more decisive for performance than insert bonding. Regarding the insert geometry, the major diameter could maximize load transfer, as this engages a larger number of reinforced struts. Regarding fastener geometry, a strategic increase in both the major diameter and the thread pitch is recommended to optimize the load-transfer mechanism. It is important to clarify that because the interface bonding is superior to the individual strut strength, failure will inherently initiate within the foam bulk regardless of the insert size. However, a larger major diameter is effective from a macro-mechanical standpoint: by expanding the effective interface area, the total number of engaged struts increases, thereby reducing the local stress intensity per individual cell wall. Consequently, while the weakest link remains a foam strut, a larger diameter shifts the global failure load to higher values by distributing the force across a broader volume of the hybrid matrix. Complementary to this, the thread pitch (and resulting undercut depth) dictates the quality of the mechanical interlocking. In cellular materials, a coarser pitch is advantageous as it prevents the mechanical degradation of individual struts during the insertion process—an issue with fine threads that tend to sever the delicate architecture of the foam framework. By utilizing a larger pitch, entire cell units can be encompassed within the thread valleys. This maximizes the volume of reinforced hybrid material that must be physically displaced or densified during pull-out, effectively leveraging the material's bulk strength through enhanced mechanical interlocking. Although larger inserts with deeper undercuts may initially seem to contradict lightweight design principles, the resulting gain in specific load-bearing capacity allows for a reduction in the total number of fasteners required for an assembly. This potentially yields a net mass saving for the overall structural system.

It must be acknowledged that due to the discrete nature of the CT scan intervals, damage evolution was captured as a series of snapshots. While the temporal resolution is insufficient to pinpoint the exact time frame of damage initiation, the comparison between pre-peak and post-peak states remains highly effective for localizing the failure of the first structural struts and tracking the subsequent spatial progression of damage.

The proposed hybrid foam system demonstrates significant potential for sustainable civil engineering applications, particularly as high-performance core materials for lightweight sandwich panels or advanced insulation elements. Due to their exceptional specific energy absorption, these materials are uniquely suited for impact and blast mitigation in critical infrastructure. Potential applications range from mobile blast barriers to high-performance protective equipment and specialized cladding designed to safeguard vehicles and sensitive devices against extreme mechanical loading.

Compared to other lightweight materials, a key advantage of the nickel-coated PU architecture is its high functional versatility, offering superior energy dissipation and tailored mechanical properties. These characteristics can be precisely tuned by adjusting the pore size of the polymer scaffold and the nickel coating thickness, allowing for a material design that is specifically optimized for various load-bearing or energy-absorbing requirements. By substituting solid metallic components with cellular hybrid structures, raw material consumption and the associated carbon footprint can be substantially reduced. This shift not only optimizes structural weight but directly supports the transition toward climate-neutral construction and resource-efficient engineering.

Despite the promising results, this study is exploratory in nature and subject to certain limitations that provide a roadmap for future research. First, the conclusions are drawn from a limited number of specimens with specific pore sizes and a single coating thickness. Since variations in these parameters are likely to affect the sensitive transition between strut failure and interfacial debonding, a broader parameter study is required to generalize these findings. Second, the observed 10–15° shear plane orientation in compression should be considered a preliminary finding; although characteristic for this material, minor misalignments or friction-induced effects inherent to the in situ compression stage cannot be entirely excluded. Furthermore, while the X-ray snapshots offer a reliable qualitative assessment of the failure sequence, the study lacks a quantitative strain analysis. Future research utilizing digital volume correlation (DVC) would provide deeper insights by precisely correlating local stress distributions with the specific coating geometry and microstructural bonding. Crucially, this will enable a direct correlation between the deformation mechanisms observed in compression and pull-out testing, allowing for a unified understanding of how the cellular architecture governs various loading scenarios. To further elucidate the mechanisms of failure initiation during pull-out, future research will incorporate high-resolution microstructural investigations such as Focused Ion Beam (FIB) milling or scanning electron microscopy (SEM) to analyze the local interface and strut damage in even greater detail. Finally, as this investigation focused on a single insert geometry, the influence of varying thread profiles remains to be evaluated. A systematic variation of geometry is expected to optimize load distribution, which will be quantified in subsequent studies. Such investigtions will be essential to developing a comprehensive design framework for the next generation of hybrid foam fasteners.

Conclusion

This study successfully demonstrated the functionality of a custom adapted in situ pull-out system designed for micro X-ray computed tomography. The integration of this experimental setup into the CT environment proves that the system is capable of capturing complex mechanical interactions within cellular hybrids under load. The setup enables three-dimensional observation of internal failure sequences such as strut facture and interfacial delamination that remain inaccessible through conventional, ex situ testing methods.

The investigation of nickel-coated polyurethane foams yielded the following main findings:

- Compression behavior: The hybrid matrix exhibits a robust mechanical response under pressure, with a collapse stress of 7.1 MPa. Failure is driven by structural inhomogeneities of the Ni-coating, resulting in localized deformation bands oriented at 10° to 15° relative to the loading axis.
- Pull-out performance: The integrated fastening system achieved a significant pull-out resistance of 4 MPa. In situ data proved that the interfacial bonding remains intact beyond the initial failure of the surrounding matrix, resulting in an annular damage zone around the insert.
- Increasing the major diameter and utilizing a coarser thread pitch of the insert were identified as primary strategies to enhance load-bearing capacity. These modifications distribute stress across a broader volume and maximize mechanical interlocking while preventing structural degradation during insertion in the manufacturing process.

Ultimately, the high specific energy absorption and functional tunability of the Ni/PU architecture underscore its potential as a sustainable material for lightweight construction and protective infrastructure in green civil engineering. This in situ CT approach establishes a robust methodological framework for future research. Future work will extend these findings by utilizing DVC to map local stress localization and by testing a larger number of specimens to ensure statistical robustness. Furthermore, systematic studies on varying pore sizes and nickel layer thicknesses, combined with numerical simulations, will provide a comprehensive basis for optimizing hybrid interfaces in impact and blast mitigation applications.

Acknowledgements

We acknowledge Fichtner & Schicht GmbH for providing the investigated foams. This work made use of the resources of the Correlative Microscopy & Tomography (CoMiTo) core facility at Saarland University. Funding for in-situ CT loading stage by German Research Foundation, grant number 316923640, is gratefully acknowledged. We acknowledge the use of ChatGPT (GPT-5.2, OpenAI) for assistance with language editing and stylistic improvement of this manuscript.

Author contributions

CRediT: **Jonas Fell**: Conceptualization, Formal analysis, Investigation, Methodology, Project administration, Validation, Visualization, Writing – original draft, Writing – review & editing; **Hendrik Jost**: Funding acquisition, Validation, Writing – original draft; **Dionne Schnubel**: Formal analysis, Investigation; **Maurice Großelindemann**: Resources, Writing – original draft; **Marius Weiler**: Methodology; **Anne Jung**: Validation, Visualization, Writing – original draft; **Hans-Georg Herrmann**: Funding acquisition, Project administration, Supervision, Writing – original draft.

Disclosure statement

The authors report there are no competing interests to declare.

Funding

This work was funded by the German Federal Ministry for Economic Affairs and Energy under Grant 03LB1011B.

ORCID

Jonas Fell http://orcid.org/0000-0002-5798-8895
Hans-Georg Herrmann http://orcid.org/0000-0003-3471-1516

References

Ashby, M. F., Evans, A., Fleck, N. A., Gibson, L. J., Hutchinson, J. W., Wadley, H. N. G., & Delale, F. (2001). Metal foams: A design guide. *Applied Mechanics Reviews*, *54*(6), B105–B106. https://doi.org/10.1115/1.1421119

Banhart, J. (2001). Manufacture, characterization and application of cellular metals and metal foams. *Progress in Materials Science*, *46*(6), 559–632. https://doi.org/10.1016/S0079-6425(00)00002-5

Bastawros, A. F., Bart-Smith, H., & Evans, A. G. (2000). Experimental analysis of deformation mechanisms in a closed-cell aluminum alloy foam. *Journal of the Mechanics and Physics of Solids*, *48*(2), 301–322. https://doi.org/10.1016/S0022-5096(99)00035-6

Betts, C., Balint, D., Lee, J., Lin, J., & Lee, P. (2014). In situ microtensile testing and X-ray microtomography-based finite element modelling of open-cell metal foam struts and sandwich panels. *The Journal of Strain Analysis for Engineering Design*, *49*(8), 592–606. https://doi.org/10.1177/0309324714539307

Bronder, S., Lorson, P., Reis, M., & Jung, A. (2025). Investigation and modelling of size effects in Ni/PU hybrid foams—A new model to predict size-effected properties in foams. *Composite Structures*, *354*, 118806. https://doi.org/10.1016/j.compstruct.2024.118806

Ceci, A., Costanza, G., Giudice, F., Sili, A., & Tata, M. E. (2025). The role of metal foams for sustainability and energy transition. *Alloys*, *4*(3), 16. https://doi.org/10.3390/alloys4030016

Fell, J., Lutter, F., Pauly, C., Engstler, M., Han, F., Costa, R., … Herrmann, H. G. (2023a). *Correlative microscopy using SEM based nano-CT* [Paper presentation]. X-Ray Nanoimaging: Instruments and Methods VI (Vol. 12698, pp. 20–29). SPIE. https://doi.org/10.1117/12.2677235

Fell, J., Pauly, C., Maisl, M., Zabler, S., Mücklich, F., & Herrmann, H. G. (2023b). Three-dimensional imaging of microstructural evolution in SEM-based nano-CT. *Tomography of Materials and Structures*, *2*, 100009. https://doi.org/10.1016/j.tmater.2023.100009

Fernandes, H., Summa, J., Daudre, J., Rabe, U., Fell, J., Sfarra, S., … Herrmann, H.-G. (2021). Characterization of ancient marquetry using different non-destructive testing techniques. *Applied Sciences*, *11*(17), 7979. https://doi.org/10.3390/app11177979

Fíla, T., Jiroušek, O., Jung, A., & Kumpová, I. (2016). Identification of strain fields in pure Al and hybrid Ni/Al metal foams using X-ray micro-tomography under loading. *Journal of Instrumentation*, *11*(11), C11017–C11017. https://doi.org/10.1088/1748-0221/11/11/C11017

Fries, M., Schäfer, F., Janka, O., Schmauch, J., & Jung, A. (2024). Influence of heat treatment on microstructure evolution and yield surfaces of Ni/PU hybrid foams. *Advanced Engineering Materials*, *26*(24), 2400235. https://doi.org/10.1002/adem.202400235

Gibson, L. J. (2000). Mechanical behavior of metallic foams. *Annual Review of Materials Science*, *30*(1), 191–227. https://doi.org/10.1146/annurev.matsci.30.1.191

Herrera-Franco, P. J., & Drzal, L. T. (1992). Comparison of methods for the measurement of fibre/matrix adhesion in composites. *Composites*, *23*(1), 2–27. https://doi.org/10.1016/0010-4361(92)90282-Y

Jung, A., & Diebels, S. (2016). Synthesis and mechanical properties of novel Ni/PU hybrid foams: A new economic composite material for energy absorbers. *Advanced Engineering Materials*, *18*(4), 532–541. https://doi.org/10.1002/adem.201500405

Jung, A., & Diebels, S. (2017). Microstructural characterisation and experimental determination of a multiaxial yield surface for open-cell aluminium foams. *Materials & Design*, *131*, 252–264. https://doi.org/10.1016/j.matdes.2017.06.017

Jung, A., & Diebels, S. (2019). Micromechanical characterization of metal foams. *Advanced Engineering Materials*, *21*(8), 1900237. https://doi.org/10.1002/adem.201900237

Jung, A., Luksch, J., Bleistein, T., Adrien, J., & Maire, E. (2018). In-situ and ex-situ micro mechanical testing of open-cell metal foams. *PAMM*, *18*(1), e201800213. https://doi.org/10.1002/pamm.201800213

Jung, A., Luksch, J., Diebels, S., Schäfer, F., & Motz, C. (2018). In-situ and ex-situ microtensile testing of individual struts of Al foams and Ni/Al hybrid foams. *Materials & Design*, *153*, 104–119. https://doi.org/10.1016/j.matdes.2018.04.075

Kaya, A. C., Zaslansky, P., Rack, A., Fischer, S. F., & Fleck, C. (2019). Foams of gray cast iron as efficient energy absorption structures: A feasibility study. *Advanced Engineering Materials*, *21*(6), 1900080. https://doi.org/10.1002/adem.201900080

Kunz, F., & Jung, A. (2022). Investigation of the structural coating homogeneity in open-porous nickel/polyurethane hybrid foams produced by flow-controlled electrodeposition. *Advanced Engineering Materials*, *24*(11), 2200262. https://doi.org/10.1002/adem.202200262

Leblanc, C., Kilingar, N. G., Jung, A., Kamel, K. E. M., Massart, T. J., Noels, L., & Béchet, E. (2022). Analysis of an open foam generated from computerized tomography scans of physical foam samples. *International Journal for Numerical Methods in Engineering*, *123*(18), 4267–4295. https://doi.org/10.1002/nme.7008

Lefebvre, L. P., Banhart, J., & Dunand, D. C. (2008). Porous metals and metallic foams: Current status and recent developments. *Advanced Engineering Materials*, *10*(9), 775–787. https://doi.org/10.1002/adem.200800241

Luksch, J., Jung, A., Pauly, C., Derr, R., Gruenewald, P., Laub, M., … Schaefer, F. (2021). Ni/Al-hybrid cellular foams: An interface study by combination of 3D-phase morphology imaging, microbeam fracture mechanics and in situ synchrotron stress analysis. *Materials*, *14*(13), 3473. https://doi.org/10.3390/ma14133473

Maurer, J., Jerabek, M., Salaberger, D., Thor, M., Kastner, J., & Major, Z. (2022). Stress relaxation behaviour of glass fibre reinforced thermoplastic composites and its application to the design of interrupted in situ tensile tests for investigations by X-ray computed tomography. *Polymer Testing*, *109*, 107551. https://doi.org/10.1016/j.polymertesting.2022.107551

Nogatz, T., Jung, A., Fíla, T., Kumpová, I., & Jiroušek, O. (2024). Analysis of the meso-mechanical deformation behavior of Al foams and Ni/Al Hybrid foams using time-lapse micro-computed tomography measurements and 3D optical flow. *Advanced Engineering Materials*, *26*(24), 2400438. https://doi.org/10.1002/adem.202400438

Pech-Can, G. E., Flores-Johnson, E. A., Carrillo, J. G., Bele, E., & Valadez-Gonzalez, A. (2024). Mechanical properties of polyurethane foam reinforced with natural henequen fibre. *Journal of Composites Science*, *8*(9), 343. https://doi.org/10.3390/jcs8090343

Reis, M., König, K., Diebels, S., & Jung, A. (2020). Micromechanical characterisation of Ni/PU hybrid foams. *Materials*, *13*(17), 3746. https://doi.org/10.3390/ma13173746

Schindelin, J., Arganda-Carreras, I., Frise, E., Kaynig, V., Longair, M., Pietzsch, T., … Cardona, A. (2012). Fiji: An open-source platform for biological-image analysis. *Nature Methods*, *9*(7), 676–682. https://doi.org/10.1038/nmeth.2019

Song, Z., Magdysyuk, O. V., Sparks, T., Chiu, Y. L., & Cai, B. (2022). Revealing growth mechanisms of faceted Al2Cu intermetallic compounds via high-speed Synchrotron X-ray tomography. *Acta Materialia*, *231*, 117903. https://doi.org/10.1016/j.actamat.2022.117903

Wang, C., & Lu, Y. (2026). Strain-variance damage modeling of microfiber-reinforced recycled cementitious composites via in-situ 4D CT and DVC. *Composites Part B: Engineering*, *310*, 113172. https://doi.org/10.1016/j.compositesb.2025.113172

Wang, C., Guo, J., Li, F., Zhang, Y., & Ma, Z. (2025). Characterization of failure modes and mechanical behavior of micro-fiber-reinforced recycled aggregate concrete under Hopkinson pressure bar and in-situ CT techniques. *Construction and Building Materials*, *458*, 139726. https://doi.org/10.1016/j.conbuildmat.2024.139726

Wang, C., Liu, J., Dai, Y., & Ma, Z. (2025). Elucidate CO2 enhancement on multiscale mechanical behavior and stiffness degradation of fiber-reinforced recycled aggregate concrete under cyclic loading. *Journal of Building Engineering*, *111*, 113298. https://doi.org/10.1016/j.jobe.2025.113298

Wang, C., Lu, Y., Zhang, Y., & Ma, Z. (2025). Sustainable carbonation-modified microfiber-reinforced cementitious composites with synergistic mechanical enhancement and 3D strain field analysis. *Construction and Building Materials*, *489*, 142416. https://doi.org/10.1016/j.conbuildmat.2025.142416

Wang, C., Lu, Y., Zhang, Y., Wu, H., & Ma, Z. (2025). Computed tomography images and digital volume correlation analysis of microstructural damage evolution in carbonated recycled aggregate concrete. *Construction and Building Materials*, *491*, 142761. https://doi.org/10.1016/j.conbuildmat.2025.142761

Wang, Y., Chen, F., Wang, X., Liu, Y., Sun, J., Gu, Y., & Yu, Y. (2023). Micro-CT in the mechanical properties and energy absorption of closed-cell aluminium foam. *Materials Today Communications*, *37*, 106962. https://doi.org/10.1016/j.mtcomm.2023.106962

Wingate, B. P., & Czabaj, M. W. (2022). In-situ imaging of flexure-induced fracture in tape-laminate composites using high-resolution X-ray computed tomography. *Composites Science and Technology*, *220*, 109288. https://doi.org/10.1016/j.compscitech.2022.109288

Wu, Y., Guo, Y., Yi, S., Lv, Z., & Fan, Z. (2024). Impact resistance of aluminum foam composites with filler and coating materials. *Polymers*, *16*(23), 3286. https://doi.org/10.3390/polym16233286

Wu, Z., Wu, S., Kruzic, J. J., Hu, Y., Yu, H., Zhang, X., … Withers, P. J. (2025). Critical damage events of 3D printed AlSi10Mg alloy via in situ synchrotron X-ray tomography. *Acta Materialia*, *282*, 120464. https://doi.org/10.1016/j.actamat.2024.120464